Coastal Environmental and Ecosystem Issues of the East China Sea,
Eds., A. Ishimatsu and H.-J. Lie, pp. 91–109.

A Tale of Two Coasts; Tidal Modification in Saemangeum and Isahaya

Seok LEE, Heung-Jae LIE, Kyu-min SONG
and Chel-Ho CHO

Korea Ocean Research and Development Institute,
1270 Sandong, Ansan 426-744, Korea

Abstract—The Saemangeum in Korea and the Isahaya in Japan have taking very similar coastal environmental change in spite of geological difference. After construction of dike in both coasts, the tidal range has decreased slightly but significantly, while the tidal current has decreased drastically. A numerical model result shows that the construction of Saemangeum dike causes the change in tidal range in whole Yellow Sea, and the change is explained as the redistribution of tidal energy from the Saemangeum to open-sea. An analytical model result shows that the construction of Isahaya dike causes the change in the resonance condition in Ariake Bay and influences on tidal system in whole Ariake Bay. The change in tidal current in both coasts is explained by the reduction of tidal prism; the volume inside the dike. The reduction of tidal current has consequently induced weakening of tidal mixing and transport of water and materials in both coasts. After the dike construction, the stratification in water column is strengthened and the turbidity has decreased significantly, eventually the phytoplankton bloom has occasionally occurred in upper layer and the oxygen deficient water has occupied in bottom layer during summer.

Keywords: Tide, Saemangeum, Isahaya, Numerical model, Analytical model, Marine environment

1. INTRODUCTION

Large scale coastal constructions like a dike cause change in bathymetry and tidal modification near the structure. There are two exemplary cases in Korea and Japan; Saemangeum Dike and Isahaya Dike, respectively. Construction of Saemangeum dike, 33-km long enclosing 401 km^2 area, in mid-western coast of Korea was started in 1991 and finished in 2006. Construction of a 7-km long sea dike to reclaim the inner part of Isahaya Bay in Ariake Bay, Kyushu, Japan, was started in 1992 and completed in 1997. Similar tidal modification feature occurs after the dike construction in both of coasts (Yanagi and Tsukamoto, 2004). Tidal range has slightly decreased and tidal current has drastically weakened after dike construction. In both of coasts with tidal range of several meters, similar change in marine environments has occurred in spite of geological difference. Study of the tidal modification mechanisms on the both

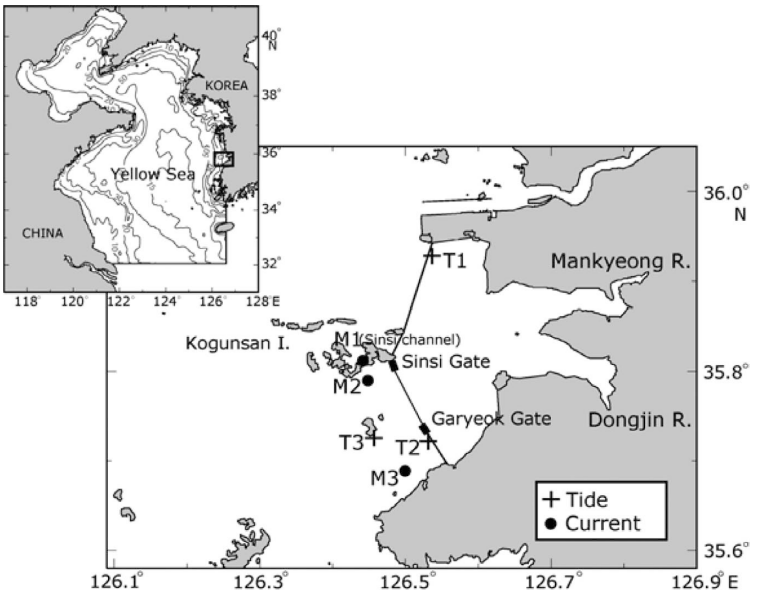

Fig. 1. Location of the study area and the Saemangeum dike, showing the three tidal monitoring stations (T1, T2, and T3) and the three current monitoring stations (M1, M2, and M3).

region is the fundamental step to understand and to predict the marine environmental change of the region.

This work is review and summary of two studies on tidal modification by dike construction in Saemangeum and Isahaya regions. Saemangeum region is almost fully opened toward Yellow Sea and 3-dimensional numerical model is used (Lee et al., 2008). Isahaya is a branch shaped bay near the end of Ariake Bay and 1-dimensional analytical model (Lee et al., 2010).

2. SAEMANGEUM REGION

Numerical model

To simulate the tidal system in the Saemangeum area, incorporation of a wetting-drying scheme is necessary. As in other areas along the western coast of Korea, the Saemangeum area originally had wide tidal flats formed by the large tidal range and gentle bottom slope structure (Fig. 1). The dike now encloses about 230 km^2 of tidal flat area, which makes up about half of the area within the dike. For this study we used a new numerical model that includes the wetting–drying scheme of Flather and Heaps (1975).

The model is based on the Princeton Ocean Model (POM; Blumberg and Mellor, 1987) and uses the same governing equations and grid system. It also uses similar procedures and splits the 2-D external mode from the 3-D internal mode. The wetting

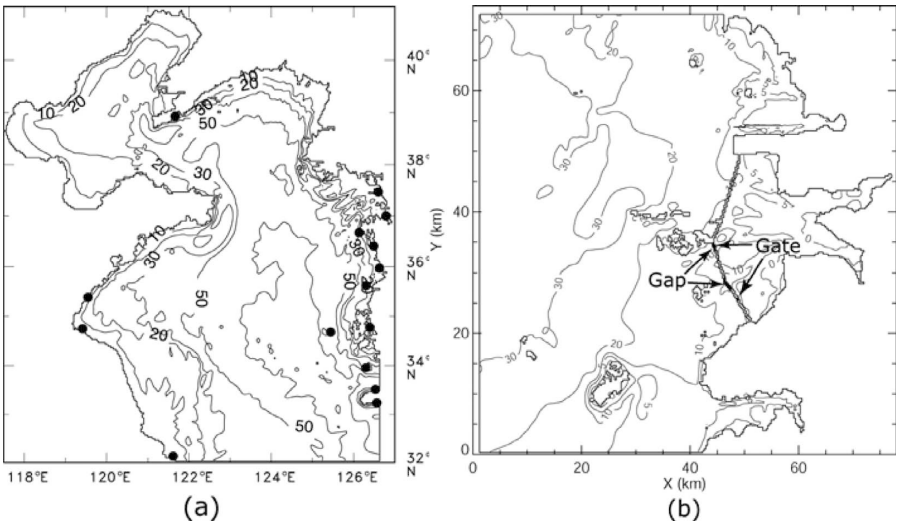

Fig. 2. Domains for the Yellow Sea model with long-term sea level stations (a) and the Saemangeum area model (b).

or drying decision is made during the calculation of the 2-D external mode. Wetting-drying schemes combined with an explicit scheme such as that of POM often create unexpected numerical oscillations (Balzano, 1998). One practical method to moderate such numerical instability is the adoption of a semi-implicit scheme for the external mode calculation (Backhaus, 1983). A semi-implicit scheme is more stable than an explicit one because high-frequency numerical oscillations are easily damped out. The semi-implicit scheme of Backhaus (1983), used in this study, consists of two time steps that have no time-splitting problem; solutions of the even and odd time steps are separated step by step, unlike the well-known leapfrog scheme, which consists of three time steps. To increase the numerical accuracy, we applied the predictor-corrector method of second-order accuracy. Each predictor and corrector step is solved by the successive over-relaxation (SOR) iteration method.

We used two kinds of model domains: the Yellow Sea domain (Fig. 2a) and the Saemangeum domain (Fig. 2b) for estimating tidal modification by the Saemangeum dike construction. The Yellow Sea domain, which includes the Bohai Sea, was bounded at 32°N to the south and 126.5°E to the east. The Yellow Sea model domain had a 1/20° × 1/20° horizontal grid and 11 vertical sigma-layers. The tidal elevation, composed of eight tidal constituents (M_2, S_2, N_2, K_1, O_1, M_4, MS_4, and MS_f), was forced on the open boundary. The Saemangeum domain model for the area near the Saemangeum dike had a horizontal grid of 300 m × 300 m and 11 vertical sigma-layers. The boundary condition of the Saemangeum domain model is interpolated from the harmonic constants calculated by the Yellow Sea domain model, and it is calibrated using observed harmonic constants in the domain.

We considered four cases according to the construction stages of the Saemangeum dike. Case Y1, in which dike construction had not begun, was used for the standard run for the Yellow Sea domain model. Dike construction was complete in Case Y2. Comparison of cases Y1 and Y2 demonstrated the Yellow Sea tidal modification caused by the dike. More detailed construction stages were modeled using the finer-resolution Saemangeum domain model. Dike construction had not begun in the standard case, Case S1. Case S2 simulated the situation just prior to dike completion in April 2006 when two open gaps remained (2.7 km wide in total). In Case S3 the dike was completed, but the two sluice gates were assumed to be continuously open, in contrast to Case S4 when the gates were operational. As mentioned above, the two sluice gates are intermittently opened to discharge fresh water or to control the water level inside the dike. For Case S4 we assumed that the gates only opened and discharged fresh water when the inside water level was higher than that outside.

Field observations

Three tidal stations were established to monitor tidal variations during the dike's construction. Anderaa WLR7 tide gauges were moored at the bottom to sample sea-level data at 10-min intervals (Fig. 1). Station T1 was the only station inside the dike; observation at this station began in July 2002. For this study we used 2 months of data collected at T1 after the dike's closure. Stations T2 and T3 were placed outside the dike; T2 was installed in January 2006, only a few months before the dike was completed; here we used data measured at T2 for the two months before dike closure. After data verification, harmonic constants for each period before and after dike closure were obtained using the TASK2000 package (Proudman Oceanographic Laboratory, Liverpool, UK). Vertical current profiles collected by an acoustic Doppler current profiler (ADCP) at the three current stations (Fig. 1) were analyzed for changes in the tidal current after the dike closure. At M2 and M3, located in the southern area outside the dike, the ADCPs were installed under a disk-type ocean surface buoy, and data sets before and after the dike's closure were examined for the months January and June 2006, respectively. Station M1 was located in the Sinsi channel, one of the channels connecting the southern and northern outside areas around the Kogunsan Islands. The ADCP at this station was installed on the sea bottom inside a trawl-resistant bottom mount (TRBM) system. The observation period at M1 was shorter than those at the other two stations, with data prior to the dike's closure available for only 17 days in December 2005. Tidal ellipse parameters of major constituents were analyzed for the vertically averaged current.

Tidal modification after the dike closure

Figure 3 shows computed tidal charts of four major constituents (M_2, S_2, K_1, and O_1) for Case Y1. The spatial pattern and location of amphidromic points coincide well with those shown on other tidal charts (Choi, 1980; Nishida, 1980). These results indicate that the computed results are meaningful and well represent the tidal system in the Yellow Sea. The computed tidal charts for Case Y2 differ slightly from those for Case Y1.

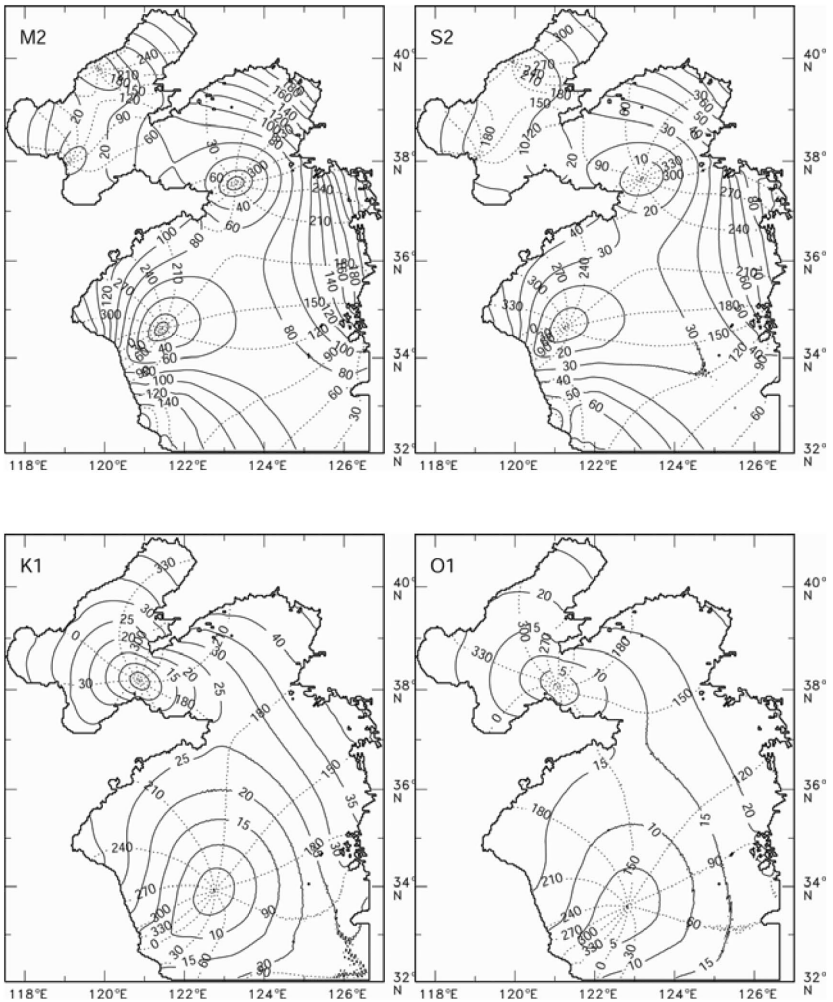

Fig. 3. Tidal charts of the four major tidal constituents computed by the numerical model.

Figure 4 shows the amplitude differences between cases Y2 and Y1 for the four tidal constituents. The contour interval is 0.5 cm and the gray shading denotes areas in which amplitude decreased after the dike closure. Amplitudes of semi-diurnal constituents (M_2 and S_2) significantly decreased, especially near the Saemangeum dike area. The maximum amplitude decreases of M_2 and S_2 outside the dike were about 10 and 4 cm, respectively, representing about 5% of the amplitudes before dike closure. However, in some other areas, the amplitude increased slightly, especially along the Chinese coast and in the northern Yellow Sea. This pattern of M2 tidal

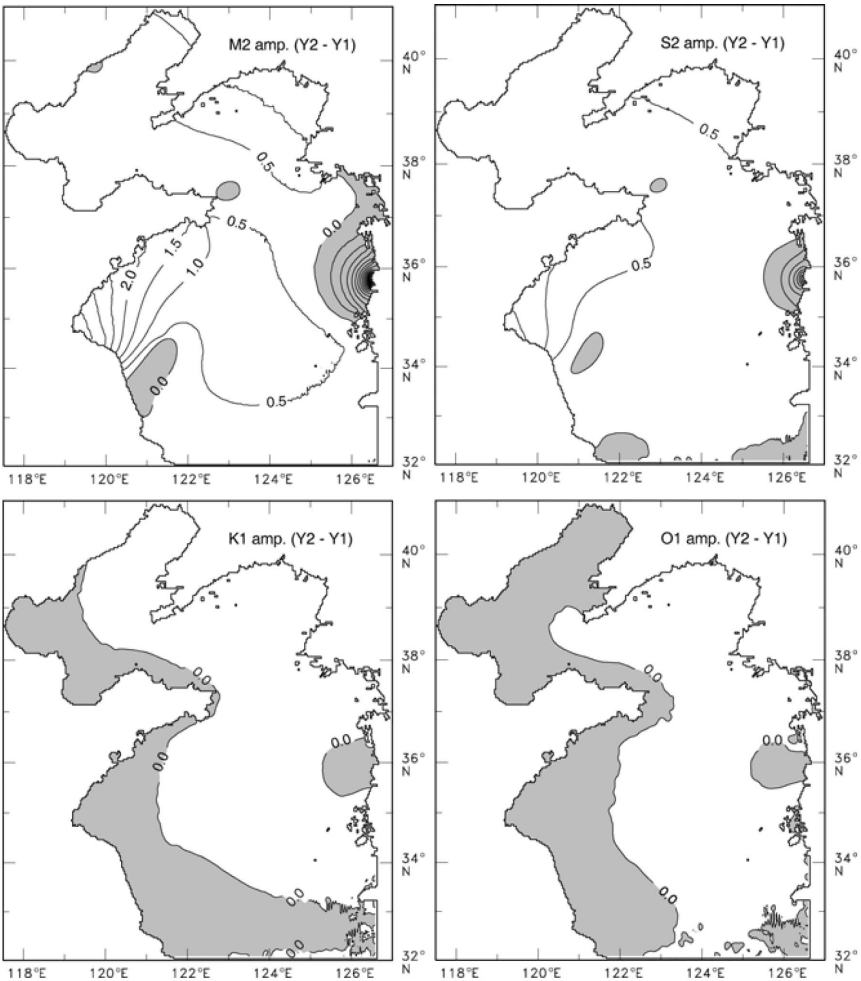

Fig. 4. Amplitude differences of four major constituents before and after dike construction. Contour interval is 0.5 cm and gray shading indicates areas where amplitudes decreased.

modification is similar to that found by Choi and Lee (2003) who reported an 8 cm maximum amplitude decrease for M_2 and a 4 cm decrease for S_2. The diurnal constituents showed completely different changes. The amplitudes of the K_1 and O_1 constituents decreased in the western Yellow Sea but increased in the easternmost part of the Yellow Sea, except for the Saemangeum area; however, the change was very small at less than 1%. The numerical model experiments indicated that only semi-diurnal tides in the Yellow Sea were significantly influenced by the Saemangeum dike construction, as discussed later.

Table 1. Comparison of tidal constants before and after dike's closure, observed at the tide monitoring stations listed in Table 2. (G: Greenwich phase)

	Period	M_2		S_2		K_1		O_1	
		H (m)	G (°)	H (m)	G (°)	H (m)	G (°)	H (m)	G (°)
T1	Before dike closure	2.22	196.3	0.85	244.5	0.34	149.0	0.26	123.2
	After dike closure	0.42	255.2	0.11	305.0	0.10	199.8	0.09	164.4
T2	Before dike closure	2.09	176.9	0.82	219.8	0.33	139.2	0.25	115.7
	After dike closure	2.05	174.3	0.77	216.8	0.34	138.9	0.27	110.0
T3	Before dike closure	2.09	178.4	0.80	221.9	0.34	139.6	0.26	113.6
	After dike closure	2.08	176.3	0.78	218.9	0.35	140.3	0.28	111.4

Because no observational data were available prior to the beginning of Saemangeum dike construction in July 2002, we could only compare the tidal harmonic constants before and after closure of the dike. Table 1 shows the changes in the four major tidal constituents caused by the dike's closure in April 2006. At T1, located inside the dike, amplitudes of M_2 and S_2 decreased by more than 80% and phases were delayed by about 60° after dike closure. This result indicates that volume transport through the two gates (total width = 540 m) was insufficient to sustain the tidal prism that existed before dike closure. At T2 and T3, located outside the dike, the amplitudes of semi-diurnal constituents decreased by 4–1 cm and phases were advanced 3–2° after dike closure. However, the amplitudes of diurnal constituents decrease by only about 2–1 cm and phases were advanced only slightly. Although the variation rate of the observed tidal amplitude is different from the computed value, the observed semi-diurnal amplitude appears to have decreased slightly, similar to the decrease shown in the numerical model results. The reason for the discrepancy is uncertain at the time of writing. More studies are needed to distinguish the net variation caused by the dike construction from that associated with natural tidal variation and to improve the boundary condition of the numerical model.

Tide modification in the Yellow Sea is associated with the transport of tidal energy. The tidal energy transport (E_i) can be approximated by harmonic constants of the surface elevation and vertical averaged currents, as follows (Pugh, 1987):

$$E_i = \frac{1}{2}\rho g H_0 \hat{u}_i \hat{\zeta} \cos\left(\theta_\zeta - \theta_{ui}\right)$$

where $\hat{u}_i$ and θ_{ui} denote the amplitude and the phase of each current component, respectively; $\hat{\zeta}$ and θ_ζ denote the amplitude and the phase of surface elevation, respectively; and ρ, g, and H_0 are water density, gravitational acceleration, and mean water depth, respectively.

An M_2 tidal wave, coming from the East China Sea, propagated northward along the western coast of Korea and then continued toward the eastern coast of China and northward to the Bohai Sea (Fig. 3). The distribution of M_2 tidal energy flux reflects

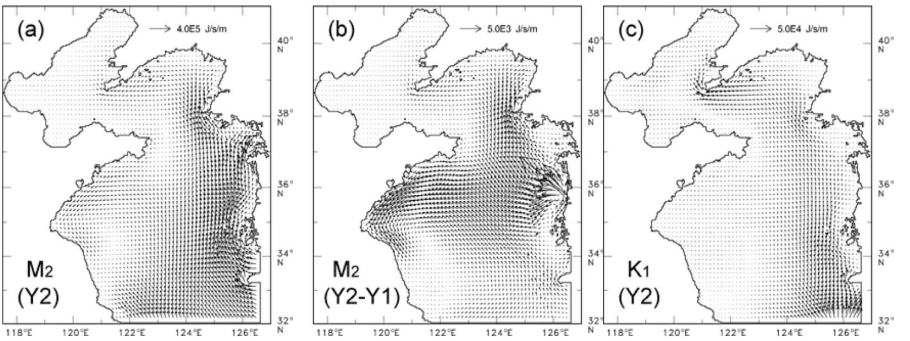

Fig. 5. Distributions of tidal energy flux. M2 tidal energy flux (a) and differences between that flux before and after dike closure (b); K1 tidal energy flux (c).

the tidal wave propagation (Fig. 5a). After the dike's closure the tidal current inside the dike vanished completely and the tidal current speed outside the dike decreased drastically, resulting in reduced energy dissipation at the sea bottom in the Saemangeum area. Due to the reduction in energy dissipation in the Saemangeum area, the net tidal energy diverged off-shore and converged along the western coast of Korea and the northern part of the Yellow Sea (Fig. 5b). The areas of divergence and convergence correspond well with areas of tidal range decrease and increase, respectively. The energy flux variations of the other semi-diurnal tides (S_2 and N_2) were similar to those for M_2. However, the diurnal tides K_1 and O_1 showed different and relatively weak energy flux variations. There was one main axis of K_1 tidal energy propagation from south to north, and its center passed about 100 km west of the center of M_2 (Fig. 5c). Therefore, because the energy propagation axis of the semi-diurnal constituents was closer to the Saemangeum area, these constituents were influenced more significantly by the dike construction.

Compared to the tidal changes, the changes in tidal currents due to the Saemangeum dike construction were both clearer and more abrupt. Figure 6a shows the computed spatial distribution of maximum flood and ebb currents for Case S1. Before the dike construction, maximum tidal current speed was greater than 50 cm/s in most of the domain. Gray shading in the figure indicates areas of strong tidal current exceeding 1 m/s. Figure 6b and c presents the ratios of maximum tidal current speeds for Cases S2 and S3, respectively, relative to those of Case S1. The dark gray areas indicate ratios greater than 100%, where the tidal currents in Cases S2 or S3 were stronger than the tidal current in Case S1. Just before the dike's closure the tidal current speed increased near the two gaps but decreased along the dike (Fig. 6b). A remarkable reduction in tidal current speed was found near both landward and seaward sides of the northern dike where no gap remained. As demonstrated in Table 2, tidal ranges were almost the same along both sides of the dike just before dike closure, indicating that there was little change in the total tidal prism at that time. This means that the tidal

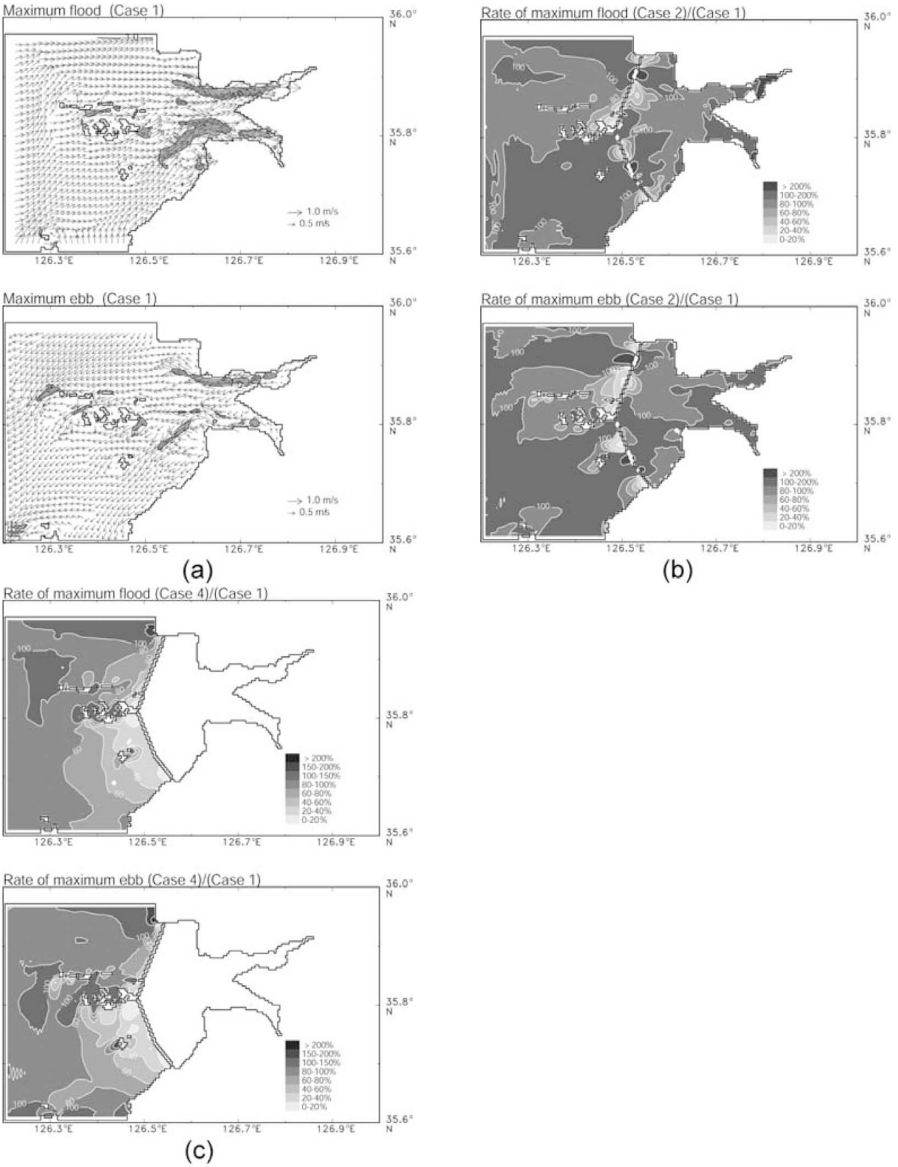

Fig. 6. Calculated maximum flood and ebb currents for Case S1 (a) and the maximum flood and ebb current speeds for Case S2 (b) and Case S3 (c) compared to those of Case S1.

current transport blocked by the dike was concentrated into the gaps in the southern part of the dike. However, after the dike was closed, the tidal current speeds decreased along the entire dike (Fig. 6c). After closure, the reduction of tidal current speed in

Table 3. Comparison of tidal ellipse parameters before and after dike's closure, observed at the current stations.

		M1		M2		M3	
		before	after	before	after	before	after
Z_0	U	8.0	–2.5	–10.4	0.6	7.8	5.0
	V	–17.9	12.4	–11.3	–2.9	1.1	0.2
M_2	Maj.	43.8	79.8	102.4	20.8	39.2	28.2
	Min.	–0.7	–1.2	6.3	4.1	1.0	1.1
	Inc.	119.0	115.8	26.8	48.4	27.4	25.1
	Pha.	100.5	3.4	17.0	21.8	3.8	22.7
K_1	Maj.	6.8	8.8	10.2	1.2	2.6	2.3
	Min.	–0.6	–0.2	–0.9	–0.3	–0.3	–0.6
	Inc.	121.2	114.0	25.4	97.4	37.8	30.8
	Pha.	158.9	181.5	184.5	189.5	192.3	217.0
M_4	Maj.	34.1	3.1	7.4	2.6	5.1	1.2
	Min.	–0.9	–2.7	1.7	–0.1	1.3	–0.6
	Inc.	119.4	137.9	48.1	100.3	26.3	93.9
	Pha.	241.8	285.7	255.8	257.4	74.4	146.5

U, V: eastward and northward components of the mean residual current.
Maj.: semi-major axis; Min.: semi-minor axis (positive value denotes counterclockwise rotation).
Inc.: incline of semi-major axis (counterclockwise from the east); Pha.: Greenwich phase.

the southern area was much larger than that in the northern one. When the gates are closed, the tidal prism vanishes in the amount of the volume change inside the dike, and the tidal current outside the dike should decrease proportionally. With the gates open, more than 80% of the tidal prism should vanish and the tidal current should decrease drastically, except near the gates. The results of tidal current observations were almost the same as the model results. Table 3 show the changes in the mean residual current and tidal ellipses after dike closure, observed at the tidal current stations. At stations M2 and M3, closing the dike weakened the tidal currents of all constituents, including the mean residual current. The M_2 semi-major axis at M2 and M3 decreased by about 80% and 30%, respectively. The rate of reduction at M2 was much larger than that at M3, which was located farther from the dike. However, at M1 in the Sinsi channel, tidal currents of semi-diurnal constituents (M_2, S_2) were strengthened while tidal currents of shallow water constituents (M_4, MS_4) were weakened. Just before the dike's closure, the shallow water components were abnormally strong and the tidal current was asymmetric in shape, with strong, short flood currents and weak, long ebb currents. After the dike closure, the shape of the tidal current became almost symmetric and the shallow water constituents declined.

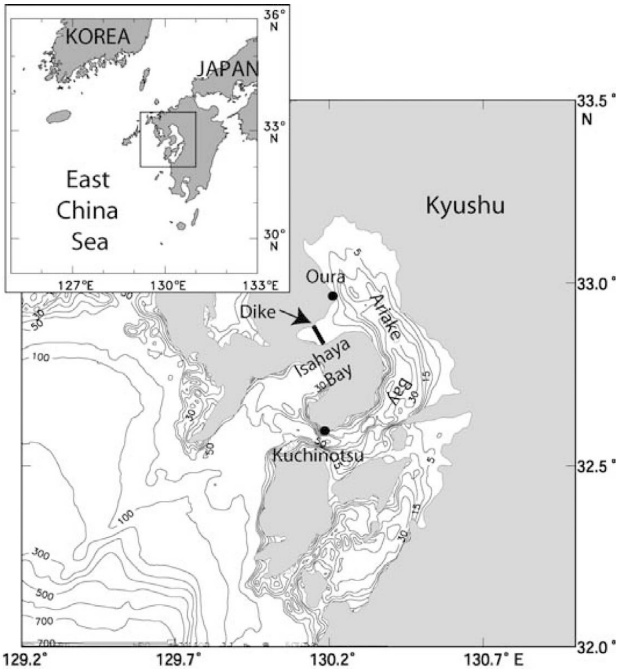

Fig. 7. Bathymetry of Ariake Bay and Isahaya Dike.

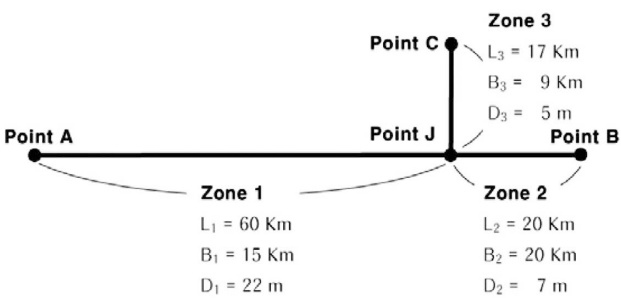

Fig. 8. Schematic diagram of simplified Ariake Bay.

3. ISAHAYA REGION

Method

Ariake Bay (shown in Fig. 7) is considered as a one-dimensional channel with one branch of Isahaya Bay near the end of the main channel. Figure 8 presents a schematic diagram of the simplified representation of Ariake Bay consisting of three

zones having constant water depth and width. Zone 1 is the main part of the bay, extending from the mouth connecting with the East China Sea (point A; Kuchinotsu) to the junction of other two zones (point J; Oura). Zone 2 is the head of the bay from point J to point B, and zone 3 is Isahaya Bay from point J to point C.

The following descriptions describe the dynamics of tides in each zone in terms of linear bottom friction (Dronkers, 1964):

$$\frac{\partial Q}{\partial t} + Ag\frac{\partial \eta}{\partial x} + \lambda Q = 0, \tag{1}$$

$$\frac{\partial \eta}{\partial t} + \frac{1}{b}\frac{\partial Q}{\partial x} = 0, \tag{2}$$

or

$$\frac{\partial^2 Q}{\partial t^2} + \lambda\frac{\partial Q}{\partial x} - gH\frac{\partial^2 Q}{\partial x^2} = 0, \tag{3}$$

where Q is the volume transport, η is the elevation from mean water depth H_0, b is a constant channel width, H ($=H_0 + \eta$) is total water depth, A ($=bH$) is the cross-sectional area of a channel, g is the gravitational acceleration, and λ is a linear bottom friction coefficient. A tidal constituent in a channel can be expressed as a single harmonic function as follows:

$$\eta = he^{iwt} + h^* e^{-iwt}, \tag{4}$$

$$Q = qe^{iwt} + q^* e^{-iwt}, \tag{5}$$

where h^* and q^* are the complex conjugates of h and q, respectively. Then, the general solutions of equations (1) and (2) in zone j can be derived easily with the small-amplitude assumption ($H_0 >> \eta$ or $H \approx H_0$) as follows:

$$q_j = q_{j1}e^{k_j x} + q_{j2}e^{-k_j x}, \tag{6}$$

$$k_j = \frac{k_j i}{wb}\left(q_{j1}e^{k_j x} - q_{j2}e^{-k_j x}\right), \tag{7}$$

where $k_j^2 = (iw\lambda - w^2)/C_j^2$, $C_j^2 = gH_{j0}$, $i = \sqrt{-1}$, and q_{j1} and q_{j2} are unknown constant complex numbers. Six boundary conditions are needed to solve equations (6) and (7) in three zones having six unknowns. The surface elevation is given at the open boundary of point A:

$$h_1(0) = h_0 = \frac{k_1 i}{wb_1}(q_{11} - q_{12}). \tag{8}$$

We assume that the ends of zones 1 and 2 (points B and C) are vertical walls without water flux:

$$q_2(L_2) = q_{21}e^{k_2 L_2} + q_{22}e^{-k_2 L_2} = 0, \tag{9}$$

$$q_3(L_3) = q_{31}e^{k_3 L_3} + q_{32}e^{-k_3 L_3} = 0. \tag{10}$$

At the junction of point J, surface elevations of the three zones must be matched, and the volume transport must be conserved as follows:

$$h_1(L_1) = h_2(0) \quad \text{or} \quad \frac{k_1 i}{w b_1}\left(q_{11}e^{k_1 L_1} - q_{12}e^{-k_1 L_1}\right) = \frac{k_2 i}{w b_2}\left(q_{21} - q_{22}\right), \tag{11}$$

$$h_1(L_1) = h_3(0) \quad \text{or} \quad \frac{k_1 i}{w b_1}\left(q_{11}e^{k_1 L_1} - q_{12}e^{-k_1 L_1}\right) = \frac{k_3 i}{w b_3}\left(q_{31} - q_{32}\right), \tag{12}$$

$$q_1(L_1) = q_2(0) + q_3(0) \quad \text{or} \quad q_{11}e^{k_1 L_1} + q_{12}e^{-k_1 L_1} = \left(q_{21} + q_{22}\right) + \left(q_{31} + q_{32}\right). \tag{13}$$

With these six boundary conditions, the particular solution in zone 1 is obtained as follows:

$$h_1 = \frac{h_0}{\alpha}\left[\cosh k_1(x - L_1) - \beta \sinh k_1(x - L_1)\right], \tag{14}$$

$$q_1 = \frac{h_0}{\alpha}\frac{w b_1}{k_1 i}\left[\sinh k_1(x - L_1) - \beta \cosh k_1(x - L_1)\right], \tag{15}$$

where $\alpha = \cosh k_1 L_1 + \beta \sinh k_1 L_1$,

$$\beta = \frac{k_1 b_2}{k_2 b_1}\tanh k_2 L_2 + \frac{k_1 b_3}{k_3 b_1}\tanh k_3 L_3. \tag{16}$$

If no other channel were connected to zone 1 ($L_2 = 0$ and $L_3 = 0$, then $\beta = 0$), the solutions of Eqs. (14) and (15) become well-known formulas for a semi-closed channel, and the surface elevation is given at the mouth of the channel (Dronkers, 1964). Solutions in zones 2 and 3 are successively obtained as follows:

$$h_j = \frac{h_0}{\alpha}\frac{\cosh k_j(x - L_j)}{\cosh k_j L_j}, \tag{17}$$

$$q_j = \frac{h_0}{\alpha}\frac{w b_j}{k_j i}\frac{\sinh k_j(x - L_j)}{\cosh k_j L_j}, \quad \text{where } j = 2, 3. \tag{18}$$

Equations (17) and (18) are the general formulas for a semi-closed channel when the surface elevation is h_0/α at the open boundary. When $x = L_1$, the surface elevation in Eq. (14) is h_0/α, which becomes the open boundary of zones 1 and 2, and the elevation at the end of the channel can be calculated as $h_0/(\alpha \cosh k_j L_j)$. The linear bottom friction coefficient λ must be specified to calculate the tide in Ariake Bay using Eqs. (14), (15), (17), and (18). Tidal energy is damped out by the bottom friction during wave propagation in a channel. The constant friction coefficient is calibrated by comparing observed harmonic constants at the mouth of Ariake Bay (Kuchinotsu)

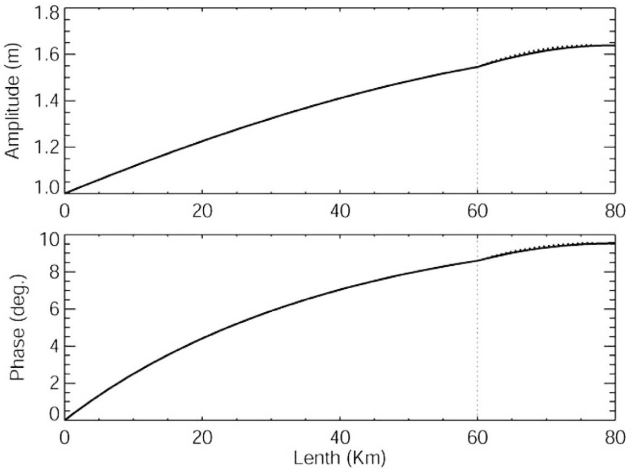

Fig. 9. Spatial distributions of the amplitude and the phase of surface elevation for the reference case.

and at the junction point (Oura). The amplitude rate has a decreasing pattern, but the phase difference is gradually delayed as the frictional effect becomes stronger. The observed amplitude of M_2 tide at the Oura is 1.55 times larger than that at Kuchinotsu, and the observed M_2 phase difference of the two points is about 8.5 degrees (Unoki, 2003). The best-matched friction coefficient is about 3.86×10^{-5} in this study.

Sensitivity and tidal modification

The calculated amplitude and phase of surface elevation at point J are 1.55 cm and 8.3 degrees, respectively. These values coincide well with observations at Oura, showing differences within 1 cm in amplitude and 1 degree in phase. We consider these results as the reference values, although we note that the channel system in Fig. 8 is a rough reflection of the bathymetry of Ariake Bay, and not enough data were used for the calibration. In the strict sense, the tidal system is sensitively dependent on channel dimensions, and uncertainty remains to some degree. After dimensions of each channel change in the 10% range and with the same friction coefficient, the amplitude and phase of elevation vary in ranges of –6.7 to 8.0% and –1.3 to 2.1 degrees, respectively. The amplitude rate and phase difference of each case can be reduced by calibrating an optimum friction coefficient. However, it is not always possible to find the optimum for all cases because the amplitude decreases and the phase is delayed when the fiction coefficient decreases. Otherwise, another combination of the dimension and the friction coefficient will exist with which the calculation is closer to the exact observed values at Oura. Although a slight mismatch remains, the reference result is sufficiently acceptable, and the analytical model with its rough approximation of the channel dimensions well reproduces the tide in Ariake Bay.

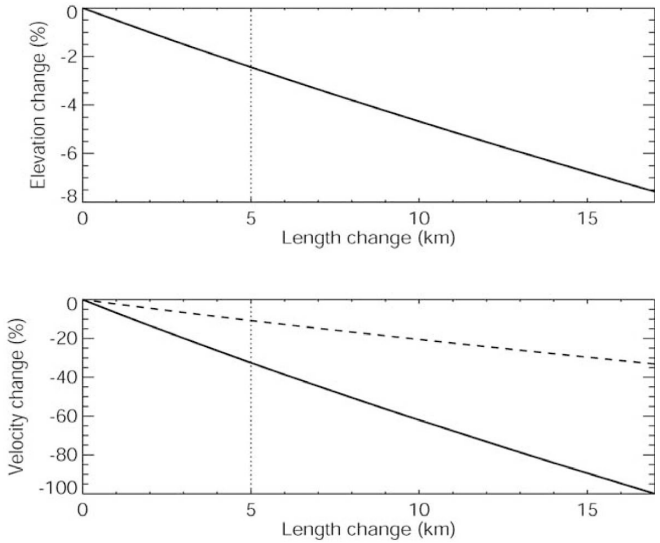

Fig. 10. Variations of the elevation amplitude and tidal current amplitude at point J with the change in the total length of zone 3. The broken line in the lower panel shows the variations of tidal current amplitude at point J toward zone 1.

Table 4. Reduction rates of elevation amplitude after the 5 km shortening of channel length of zone 3 for cases of 10% change in channel dimension.

		Zone 1	Zone 2	Zone 3
Length	+10%	–2.82	–2.48	–2.74
	–10%	–2.10	–2.40	–2.15
Width	+10%	–2.17	–2.48	–2.69
	–10%	–2.78	–2.40	–2.19
Depth	+10%	–2.15	–2.44	–2.42
	–10%	–2.82	–2.44	–2.46

Figure 9 shows the spatial distribution of the amplitude and the phase of surface elevation for the reference case. The amplitude of the elevation shows a pattern of gradual increase from the mouth to the end of the channel, while the phase is gradually delayed. Using the same boundary and friction coefficient, we calculate the tidal change in Ariake Bay after the construction of Isahaya Dike, which decreased the channel length of zone 3 by about 5 km. The amplitude of M_2 at point J becomes gradually smaller when the length of zone 3 is decreased from 17 km to zero (Fig. 10). When zone 3 is reduced to 12 km in length, the elevation amplitude decreases by about 2.4%, and the tidal current amplitude decreases by about 32.5% at the mouth of

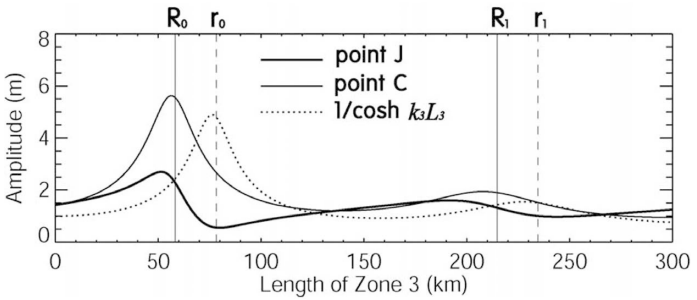

Fig. 11. Changes in elevation amplitudes at point J (thick solid curve) and point C (thin solid curve) with change in the total length of zone 3. The dotted curve is the calculated value of $1/\cosh k_3 L_3$. Vertical solid and broken lines denote resonance lengths calculated by Eqs. (22) and (21), respectively.

zone 3. The tidal current speed at the end of the channel must be zero, and it is almost proportional to the distance from the end of the channel within a short range. Therefore, the tidal current is much more influenced by the shortening of the channel in the short range. At point J, the surface elevations are reduced at equal rates for the three channels, but the tidal currents show different rates of reduction in each channel. In zone 2, the tidal current reduction is relatively weak in the whole channel and almost the same as the reduction in elevation at point J at the mouth of zone 2. The tidal current reduction rate at point J toward zone 1 is about 10.8%, which is the weighted mean of transport reduction in the other two channels. This calculated value corresponds well with observed and two-dimensional numerical model results by Unoki (2003), who found that the tidal current decreased by about 10–30% near the mouth of Isahaya Bay after the construction of Isahaya Dike.

Table 4 shows the decreasing rates of the elevation amplitude at point J with 5 km shortening of zone 3 when each dimension of the channel system changes in the 10% range. In all cases, decreases in rates were in the range of 2.1–2.8%. Therefore, we can conclude that the 5-km shortening of the channel length caused obvious weakening of the tidal system, despite the uncertainty of the channel dimensions.

Resonance condition

Shortening a channel does not always cause tidal weakening. For example, the tidal elevation of M_2 was amplified after the construction of a sea dike in the Mokpo coastal zone in Korea (Kang, 1999). The characteristics of these tidal modifications can be explained by the resonance condition of the channel system. We can expect two resonance conditions in the three-channel system in Eqs. (14), (15), (17), and (18):

$$\alpha = \cosh k_1 L_1 + \left(\frac{k_1 b_2}{k_2 b_1} \tanh k_2 L_2 + \frac{k_1 b_3}{k_3 b_1} \tanh k_3 L_3 \right) \sinh k_1 L = 0, \tag{19}$$

$$\cosh k_j L_j = 0, \quad \text{where } j = 2,3. \tag{20}$$

Equation (20) without a friction gives the well-known resonance length in a semi-enclosed channel. The traditional resonance length in a single channel (i.e., 1/4 wavelength of an M2 tidal wave) of zone 3 (r) is as follows:

$$r_N = \frac{\pi(2N+1)}{2}\frac{C_3}{w}, \quad \text{where } N = 0,1,2,\ldots. \tag{21}$$

Similarly, equation (19) gives another resonance length. The new resonance length by the complex effect of the three-channel system (R) is as follows:

$$R_N = \frac{C_3}{w}\left\{\tan^{-1}\left[\frac{C_1 b_1}{C_3 b_3}\cot\left(L_1\frac{w}{C_1}\right) - \frac{C_2 b_2}{C_3 b_3}\tan\left(L_2\frac{w}{C_2}\right)\right] + \pi N\right\},$$
$$\text{where } N = 0,1,2,\ldots. \tag{22}$$

Figure 11 shows changes in elevation amplitudes at points J and C with change in the total length of zone 3. The figure also shows the calculated value of $1/(\cosh k_3 L_3)$, which is independent of location, and the vertical resonance lengths calculated by Eqs. (22) and (21). The minimum resonance length by the complex effect (R_0) is about 56 km, which is shorter than the resonance length in a single channel (r_0 = 78 km). The amplitude at point J is almost maximum when the length of zone 3 is R_0, and the value of $1/(\cosh k_3 L_3)$ is almost maximum when the length of zone 3 is r_0. These maxima are not exactly matched with the resonance lengths calculated by Eqs. (21) and (22) because of the frictional effect (Dronkers, 1964). It is remarkable that the maxima amplitudes at point C do not occur when the channel length of zone 3 is about r_0, the condition at which the amplitude at point J reaches its minimum. This means that the actual resonance condition in this channel system is controlled only by Eq. (19).

Open-boundary condition

As mentioned above, in our calculation, the open boundary condition at point A is fixed at 1-m elevation amplitude and 0 degrees phase, but observations showed that the amplitude at Kuchinotsu decreased by 1.3% after the construction of Isahaya Dike. The dike may have some effect on the tidal variation at Kuchinotsu; however, it is hard to quantitatively separate the amplitude decrease into an inner effect of Isahaya Dike construction and an outer effect of open-ocean tidal variation. The amplitude variation at the open boundary has to cause almost the same rate of variation in the whole inner area in the linear system. When the amplitude at point A decreases 1.3% and the length of zone 3 is shortened by 5 km, the amplitude at point J decreases by 3.7% which is slightly larger than the observed 3.4% decrease at Oura and similar to the summed decrease of 2.4% caused by zone 3 shortening with a fixed open-boundary condition and variation of the open boundary.

If natural variability and noise in the observation are ignored and our calculation is supposed to be real, we can conclude that at least 50% of the elevation amplitude decrease at the inside area near Oura is caused by Isahaya Dike. Variation of the open-boundary tide has a secondary effect on tidal modification in Ariake Bay.

4. CONCLUSION AND DISCUSSION

Constructions of dike in both region have induced similar tidal modification feature. Saemangeum dike has influenced the tides and tidal currents not just near the dike but throughout the Yellow Sea. Amplitudes of semi-diurnal constituents decreased significantly after dike constructions but diurnal constituents were very weakly influenced. The difference reflects the differences in tidal energy propagation patterns. The tidal energy propagation axes of semi-diurnal constituents are closer to the Saemangeum area than those of diurnal constituents; thus, the semi-diurnal constituents are more sensitive to the influences of dike construction. Isahaya dike also has influenced on tidal system in whole Ariake Bay. The resonance condition in equation (19) affected the tidal characteristics more effectively and substantially than did the traditional resonance condition in equation (20). The tide in Ariake Bay could be most vigorous and the elevation amplitude at Oura could become about 2.8 times that at Kuchinotsu, when Isahaya Bay had the optimum length of 50 km. This means that the tide in Ariake Bay should become weaker as the length of Isahaya Bay decreases from the optimum length.

Dynamics of change in tidal range in both regions are explained in different way. However, the reason of changes in tidal current are obvious and same; the construction of dike which causes reduction of tidal prism. The tidal current plays an important role in the marine environment in both regions and has been reduced drastically since closure of the dike walls. Weakening of the tidal currents has led to abrupt changes in the marine environment since the dike's completion. After Saemangeum dike construction, the sea surface temperature near the dike has change (Yoon et al., 2009) and the suspended sediment concentration has decreased (Min et al., 2006) and plankton blooms have occasionally occurred since the dike's closure (Lie et al., 2008). These effects are similar to those observed in the Ariake Bay following the closure of the Isahaya dike (Matsuno and Nakata, 2004; Nakata, 2005; Ishizaka et al., 2006). To understand coastal marine environments, we must have a good understanding of the characteristics of tidal systems. Methods presented here can be used to provide general information on tides in a channel system.

REFERENCES

Backhaus, J. O., 1983. A semi-implicit scheme for the shallow water equations for application to shelf sea modeling. *Continental Shelf Research*, **2**(4), 243–254.

Balzano, A., 1998. Evaluation of methods for numerical simulation of wetting and drying in shallow water flow models. *Coastal Engineering*, **34**, 83–107.

Blumberg, A.F. and G.L. Mellor. 1987. A description of three-dimensional coastal ocean circulation model. p.1-16. In: Three-dimensional coastal ocean models. ed. by N.S. Heaps. AGU.

Choi, B. H., 1980. A tidal model of the Yellow Sea and Eastern China Sea. KORDI, BSPI 00019(3)-36-2, Seoul, 72 pp. (in Korean with English abstract)

Choi, B. H. and H. S. Lee, 2003. Preoperational simulation of dike closure for Saemangeum tidal barriers. Proceeding of Workshop on Hydro-environmental Impacts of Large Coastal Developments. May 21–23, 2003. Seoul, Korea.

Dronkers, J. J., 1964. Tidal computations in rivers and coastal waters. North-Holland Publishing Co., Amsterdam, P. 516.

Flather, R. A. and N. S. Heaps (1975): Tidal computations for Morecambe Bay. *Geophys. Journal of Royal Astronomical Society*, **42**, 489–517.

Ishizaka, J., Y. Kitaura, Y. Touke, H. Sasaki, H. Murakami, T. Suzuki, K. Matsuoka, and H. Nakata, 2006. Satellite detection of red tide in Ariake Sound, 1998-2001. *Journal of Oceanography*, **62**, 37–45.

Kang, J. W., 1999. Changes in tidal characteristics as a result of the construction of sea-dike/sea-walls in the Mokpo coastal zone in Korea. *Estuarine, Coastal and Shelf Science*, **48**(4), 429–438.

Lee, S., H.-J. Lie, K.-M. Song, C.-H. Cho, and E.-P. Lim, 2008. Tidal modification and its effect on sluice-gate outflow after completion of the Saemangeum Dike, South Korea. *Journal of Oceanography*, **64**, 763–776.

Lee, S., H.-J. Lie, K.-M. Song, S.-T. Jang and C.-H. Cho, 2010. Analytical Model of Tidal Modification in Ariake Bay, Japan. (Submitted for publication)

Lie, H.-J., C.-H. Cho, S. Lee, E.-S. Kim, B. J. Koo, and J. H. Noh, 2008. Changes in marine environment by a large coastal development of the Saemangeum reclamation project in Korea. *Ocean and Polar Research*, **30**, 475–484.

Matsuno T. and H. Nakata, 2004. Physical processes in the current fields of Ariake Bay. *Bulletin on Coastal Oceanography*, **25**(1), 11–17. (in Japanese with English abstract)

Min, J.-E., J.-H. Ryu, Y.-H. Ahn, and K.-S. Lee, 2006. Development of Suspended Sediment Algorithm for Landsat TM/ETM+ in coastal sea water. *Korean Journal of Remote Sensing*, **22**(2), 87–99. (in Korean with English abstract)

Nakata, H., 2005. Recent environmental change and its implication for the production system of Ariake Bay. Proceedings of the Symposium on Tidal Flat Environments in East Asia: Present and Perspective, Oct. 2005. Nagasaki, 11–18.

Nishida, H., 1980. Improved tidal charts for the western part of the North Pacific Ocean. Report of Hydrographical Research, 15.

Pugh, D. T., 1987. Tides, Surges and Mean Sea Level. Bath Press, Avon, England, 472 pp.

Unoki, S., 2003. Why did the tide and tidal current decrease in Ariake Bay? *Oceanography in Japan*, **12**(1), 85–96. (in Japanese with English abstract)

Yanagi, T. and H. Tsukamoto, 2004. Year-to-year variation in tidal amplitude in Ariake Bay. *Oceanography in Japan*, **12**, 295–300. (in Japanese with English abstract)

Yoon, S., J.H. Ryu, J.-E. Min, Y.-H. Ahn, S. Lee and J.-S. Won, 2009. Monitoring of the Sea Surface Temperature in the Saemangeum Sea Area Using the Thermal Infrared Satellite Data. *Korean Journal of Remote Sensing*, **25**(4), 339–357.

S. Lee (e-mail: lees@kordi.re.kr), H.-J. Lie, K. Song and C.-H. Cho